Effect of the size-induced structural transformation on the band gap in CdS nanoparticles

2000 J. Phys.: Condens. Matter 12 10647

(http://iopscience.iop.org/0953-8984/12/50/325)

J. Phys.: Condens. Matter **12** (2000) 10647–10654. Printed in the UK PII: S0953-8984(00)16664-0

Effect of the size-induced structural transformation on the band gap in CdS nanoparticles

R Banerjee, R Jayakrishnan† and P Ayyub

Department of Condensed Matter Physics and Materials Science,
Tata Institute of Fundamental Research, Mumbai 400005, India

Received 24 August 2000, in final form 25 October 2000

Abstract. The interrelation between particle size, crystal structure and optical properties in semiconductor quantum dots has elicited widespread interest. We report the first attempt at relating the size-induced transformation from a hexagonal to a cubic structure in CdS nanoparticles to a change in the band gap. CdS nanoparticles with particle size in the 0.7–10 nm range were prepared by chemical precipitation using thiophenol as a capping agent. Whereas the band gap for bulk hexagonal CdS is about 2.5 eV, that for 1 nm cubic CdS nanoparticles was found to be almost 3.9 eV. We also suggest a simple mechanism (based on the periodic insertion of stacking faults) for the transformation from the cubic zinc blende structure to the hexagonal wurtzite structure.

1. Introduction

Currently, there is great interest in the optical and transport properties of nanometre-sized semiconductor particles or quantum dots [1]. These show significant departures from bulk optical and electronic properties when the scale of confinement approaches the excitonic Bohr radius (r_B), which sets the length scale for optical processes [2]. Quantum dots of II–VI semiconductors have attracted particular attention, because they are relatively easy to synthesize in the size range required for quantum confinement. These materials are of potential interest in non-linear optics and in fast optical switching [3]. Nanocrystalline CdS, CdTe, CdSe, ZnSe and PbS have been synthesized by a variety of methods including precipitation, sputtering, electrochemical deposition and inverse micelles. A reduction in the particle size strongly influences the crystallinity, melting point and structural stability. We need to understand how these aspects affect optoelectronic properties.

Cadmium sulphide is a wide band gap semiconductor with $E_g \approx 2.5$ eV [4]. It is used in photodetectors and for solar cell applications as n-type window layers in heterojunction devices [5]. The optical properties of CdS have been extensively studied [6, 7]. Quantum size effects are quite pronounced because CdS has a rather large r_B (≈3 nm) [1]. CdS nanoparticles are attractive candidates for optoelectronic applications as it is possible to engineer the band gap over a wide spectral range (visible to UV).

Bulk CdS has a hexagonal wurtzite-type (W) crystal structure with $a = 0.4160$ nm and $c = 0.6756$ nm [8]. Two other structures (see table 1) are observed *only* in nanocrystalline CdS [8]: (a) a cubic zinc blende (Z) phase under ambient conditions, and (b) a high-pressure rocksalt phase [9]. The wurtzite to rocksalt transformation involves not only a change in symmetry (hexagonal to cubic) but also a change in the nearest-neighbour atomic coordination

† Current address: Department of Materials and Interfaces, Weizmann Institute of Science, Rehovot, Israel.

0953-8984/00/5010647+08$30.00

Table 1. Structure data for the three known crystallographic phases of CdS [8].

Structure type	Crystal system	Space group	Lattice parameters (nm)	Atom positions
Wurtzite (2H)	Hexagonal	$P6_3mc$	$a = 0.4160$ $c = 0.6756$	Cd $(0.333, 0.667, 0)$ S $(0.333, 0.667, 0.375)$
Zinc blende (3C)	Cubic	$F\bar{4}3m$	$a = 0.5832$	Cd $(0, 0, 0)$ S $(0.25, 0.25, 0.25)$
Rocksalt	Cubic	$Fm\bar{3}m$	$a = 0.5420$	Cd $(0, 0, 0)$ S $(0.5, 0.5, 0.5)$

(from four to six), whereas the wurtzite to zinc blende transformation involves only a change in symmetry. The two types of transition are affected by particle size in different ways. High-pressure studies show that as the particle size decreases, the critical pressure at which CdS and CdSe transform from the wurtzite to the rocksalt structure increases [9]. Again, as the size of CdS nanoparticles decreases, the equilibrium crystal structure tends to change from the hexagonal W type to the cubic Z type. The size dependence of the structural stability in CdS is one of the subjects of the present study.

The cubic (Z) phase has been observed [3] in chemically synthesized 3 nm CdS nanoparticles and the structure became hexagonal (W) above 300 °C. The authors suggest that the cubic phase is either: (i) a non-equilibrium (metastable) phase that transforms to the stable hexagonal phase on annealing, or (ii) an equilibrium phase for CdS *nanoparticles*. The latter implies that the cubic to hexagonal transition on heating is a size-driven one caused by sintering and grain growth. Experimentally, it is difficult to distinguish between the two models since annealing cubic CdS nanoparticles would result both in coarsening as well as thermally induced structural relaxation. Also, the authors observed the hexagonal phase only on heating and not in any of their as-precipitated samples.

In x-ray diffraction (XRD) experiments, it may be difficult to detect the size-driven structural transition due to the Scherrer broadening [10] in nanoparticles. The other complicating factor is the considerable overlap between the XRD lines of the hexagonal and cubic structures. Nanda *et al* [11] observed the hexagonal phase in 4.5 nm CdS particles, but could not conclusively identify the structure of the 2.5 nm particles, and suggested a possible mixture of hexagonal and cubic phases. In contrast, Herron *et al* [12] have indexed similar-looking XRD patterns from 1.5–3.5 nm CdS nanoparticles to a single cubic phase with two broad peaks.

Using high-resolution electron microscopy (HREM), Ricolleau *et al* [13, 14] studied the structure of CdS nanoparticles prepared by the inverse micelle technique. They observed the cubic (Z) structure ($a = 0.582$ nm) when $d < 4$ nm, and the hexagonal (W) structure for $d > 6$ nm. For intermediate sizes, they observed either the Z-type phase with stacking faults and twin boundaries which locally gave rise to the W-type phase, or a two-phase mixture within the *same* particle with both cubic and hexagonal domains sharing their close-packed planes at the boundary [14]. Most of the above results indicate that a size induced hexagonal to cubic transformation occurs in CdS at $\approx$4 nm. Note that this is also the size regime in which quantum confinement is expected. However, the possibility of a change in the band gap accompanying the size-induced structural transition in CdS does not appear to have been addressed so far. Here we report a detailed study of the mechanism of the structural transition in CdS nanoparticles as a function of particle size, as well as the influence of the change in crystal structure on the band gap.

2. Experimental procedure

CdS nanoparticles were synthesized via precipitation from an aqueous solution containing cadmium chloride, thiourea and ammonia, by a process used for the fabrication of solar cells comprising of CdTe and $CuInSe_2$ thin films [15]. Measured quantities of $CdCl_2$ and NH_4Cl were added to an aqueous bath maintained at 65 °C and dissolved by continuous magnetic stirring. The capping agent, thiophenol was then added to the solution. The pH of the mixture was raised to 7.5 by adding NH_4OH. Precipitation was achieved by adding a measured quantity of thiourea and the reaction was allowed to proceed for ∼30 min. The presence of thiophenol arrests the agglomeration of the CdS particles during precipitation. Further, since thiophenol forms a coating on the surface of the CdS nanoparticles, it effectively reduces the heterogeneous nucleation of new particles on the surface of existing ones, thus reducing the precipitation rate.

The precipitate was separated from the aqueous solution by centrifuging at 8000 rpm. The separated nanoparticles were repeatedly washed in methanol to remove traces of thiophenol and unreacted chemicals. After drying, some portion of the CdS sample was dispersed in DMSO (dimethyl sulphoxide) to form a stable suspension for spectroscopic studies. The dispersion was ultrasonically agitated to break up any CdS agglomerates, which might have formed during centrifuging and drying. For XRD studies, a part of the sample was dispersed on a glass slide with collodion. The chemical reaction that results in the precipitation of CdS nanoparticles can be represented as:

$$Cd(NH_3)_4^{2+} + SC(NH_2)_2 + 2OH^- \rightarrow CdS + H_2CN_2 + 4NH_3 + 2H_2O \qquad (1)$$

The quantities of the reactants used are as follows: (1) M/50 $CdCl_2$ and M/15 NH_4Cl added to 100 ml distilled water, (2) different quantities of thiophenol solution (1% v/v in methanol) were used to obtain particles of different average size, (3) M/7 thiourea was added for the precipitation of CdS nanoparticles.

X-ray diffraction studies were carried out in a Siemens D500 diffractometer, using Cu Kα radiation. The mean particle size (coherently diffracting domain size) was estimated from the FWHM of the diffraction lines using the Scherrer formula [10] after removing the contribution of the Kα_2 component by the Rachinger method [16]. The slit widths used were 1° (scatter) and 0.05° at the detector. The scan step size was 0.02° and the collection time was 4 s/step. The optical absorption was recorded in a Shimadzu spectrophotometer in the wavelength range 200–800 nm, measurements being carried out at intervals of 0.5 nm. The path length in the quartz cells was 1 cm.

3. Results

3.1. Structural transformation

Here we discuss XRD results from four of the nanoparticle CdS samples (CdS-I, CdS-II, CdS-III and CdS-IV) synthesized using the above technique. The samples differ only in the amounts of thiophenol used: from 0.5 ml in the case of CdS-I to 1.5 ml in the case of CdS-IV. Expectedly, larger quantities of capping agent lead to smaller particle sizes.

The XRD pattern from CdS-I (see figure 1) can be consistently indexed on the basis of the hexagonal, W-type structure, in which the six prominent lines correspond to the reflections $(10\bar{1}0)$, (0002), $(10\bar{1}1)$, $(11\bar{2}0)$, $(10\bar{1}3)$ and $(11\bar{2}2)$. The weak $(10\bar{1}2)$ peak was also observed. The estimated x-ray size for this sample was ∼10 nm based on the FWHM of the $(11\bar{2}0)$ peak. The XRD spectrum from CdS-II apparently exhibits only two broad peaks, centred at $2\theta \approx 27°$ and $2\theta \approx 47°$, but a more careful study of the pattern suggests that these two peaks are overlaps of multiple peaks. This is also indicated by the marked asymmetry of the peak

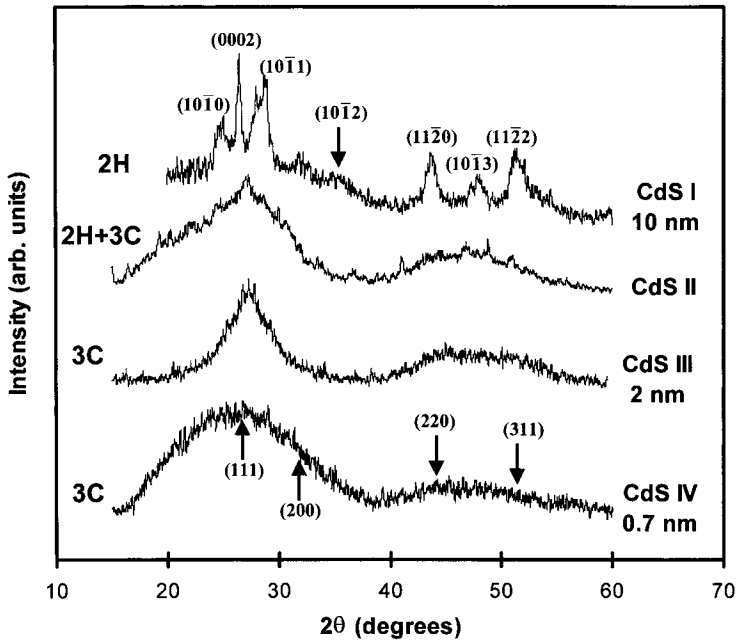

Figure 1. X-ray diffraction spectra from CdS samples with different average particle size (Scherrer size). The XRD pattern from CdS-I is indexed on the basis of the hexagonal ($2H$) wurtzite structure, while that of CdS-IV has been indexed with respect to the cubic ($3C$) zinc blende structure.

Table 2. A summary of the crystal structure and optical absorption data for CdS nanoparticles. Band gaps calculated from absorption edges for the four samples are listed. Note that there are two band gaps for the CdS-II sample, resulting from a mixture of hexagonal and cubic phases present in the sample.

Sample	Band gap (eV) E_g	Size (nm) from E_g	Size (nm) from x-ray	Crystal structure
CdS I	2.59	9.0	10	hexagonal
CdS II	2.76	5.2 (h)		hexagonal
	3.54	4.5 (c)		+ cubic
CdS III	3.57	2.0	2	cubic
CdS IV	3.85	0.7	0.7	cubic

centered at 27°, resulting from the overlap of the (10$\bar{1}$0), (0002), and (10$\bar{1}$1) peaks of the hexagonal (W) structure. The increased overlap in CdS-II is clearly a result of line broadening due to the smaller particle size in this sample as compared to CdS-I. Note, however that the two most prominent peaks for cubic CdS with a Z-type structure also occur close to 27° (111) and 44° (220). Thus, the presence of a cubic phase in CdS-II cannot be ruled out based on XRD data, but the majority phase in this sample is certainly the hexagonal phase (as indicated by the asymmetric peak broadening). Estimation of the mean x-ray size is not possible for CdS II due to the peak overlaps as well as the possible presence of a mixture of cubic and hexagonal phases.

We now consider the XRD pattern from CdS-III. Again there are only two broad peaks centered at $2\theta \approx 27°$ and $2\theta \approx 47°$ (figure 1), but there are two important differences between the diffraction patterns of CdS-II and CdS-III. In CdS-III the width of the peak at $\approx$27° is significantly smaller, and it is much more symmetric. These observations indicate that the 27°

peak in CdS-III is a single line and not an overlap of multiple lines. It can be identified as the (111) line (relative intensity, $I/I_0 = 100\%$) of the cubic Z phase. The reduction in the width of this peak despite a decrease in particle size is a definite indicator of the change in crystal structure from hexagonal to cubic. The second broad peak in CdS-III is an overlap of the cubic (220) peak at $\approx 44^\circ$ ($I/I_0 = 80\%$) and the cubic (311) peak at $\approx 52^\circ$ ($I/I_0 = 60\%$). The mean x-ray size for the CdS III sample, calculated from the FWHM of the (111) peak, is $\sim$2 nm. The nature of the XRD pattern for CdS IV is similar to that of CdS III, but the width of both lines is significantly larger. The mean particle size for this sample is $\sim$0.7 nm. Table 2 lists the crystal structures and mean particle sizes derived from the x-ray diffraction data, for the different samples of CdS nanoparticles.

3.2. Optical absorption

The optical absorption data for CdS-I, CdS-II, CdS-III and CdS-IV are shown in figure 2. The absorption edge corresponding to the band gap in bulk hexagonal W-type CdS is indicated by an arrow. It is evident from figure 2 that all four samples exhibit absorption edges which are blue-shifted with respect to the bulk CdS band gap, arising from quantum confinement effects in the nanoparticles. Note that there are two distinct absorption edges in CdS-II: one at $\lambda \approx 450$ nm and the other at $\lambda \approx 350$ nm. This is a unique feature of this sample, as all others exhibit a single absorption edge. The band gaps corresponding to the absorption edges for all four CdS samples are listed in table 2. The band gap of bulk hexagonal W-type CdS is $\approx$2.5 eV. The blue-shift in the band gap in nanoparticles due to quantum confinement has the quantitative form [17]:

$$\Delta E_g \equiv E_g^{\text{nano}} - E_g^{\text{bulk}} = \frac{\hbar^2 \pi^2}{2MR^2} \tag{2}$$

where R is the radius of the particle and M is the effective mass of the system. For hexagonal CdS, $M = 1.919 \times 10^{-31}$ kg. Since CdS-I exhibits a hexagonal structure, equation (2) could be used to estimate the particle size, using the observed blue-shift in the band gap, $\Delta E_g = 0.09$ eV. The corresponding particle diameter is 9 nm, which is in very good agreement with the x-ray size (10 nm).

The bulk band gap and the effective mass are unknown for the cubic Z phase of CdS. So, the optical absorption data for CdS-III and CdS-IV, both of which consist of single phase cubic CdS, were fitted to a simplified form of equation (2):

$$\Delta E_g = \frac{A}{R^2} \tag{3}$$

where A is a constant which depends on the effective mass (M). The resulting value of the band gap for the *bulk* cubic Z phase of CdS is $E_g^{\text{cubic}} = 3.53$ eV. This is only a notional value since the cubic phase may never exist in the bulk.

The situation is a little more complex in CdS II, which is a mixture of the cubic and hexagonal phases and consequently exhibits two distinct absorption edges. The band gap corresponding to each absorption edge is given in table 2. It is important to assign the band gaps correctly to the two phases and check for overall self-consistency. Since the band gap of the bulk hexagonal phase ($\sim$2.5 eV) is smaller than the band gap for the 'bulk' cubic phase ($\sim$3.5 eV), the smaller of the two band gaps in CdS II was assigned to the hexagonal phase and the larger to the cubic phase. The corresponding particle diameters, obtained from equation (2), for the hexagonal and cubic phases are 5.2 nm and 4.5 nm, respectively. Thus, the particle size distribution in CdS-II is quite small, which is consistent with the fact that the other CdS samples (I, III and IV) prepared by the same technique, consisted of a single phase, suggesting a relatively small size distribution.

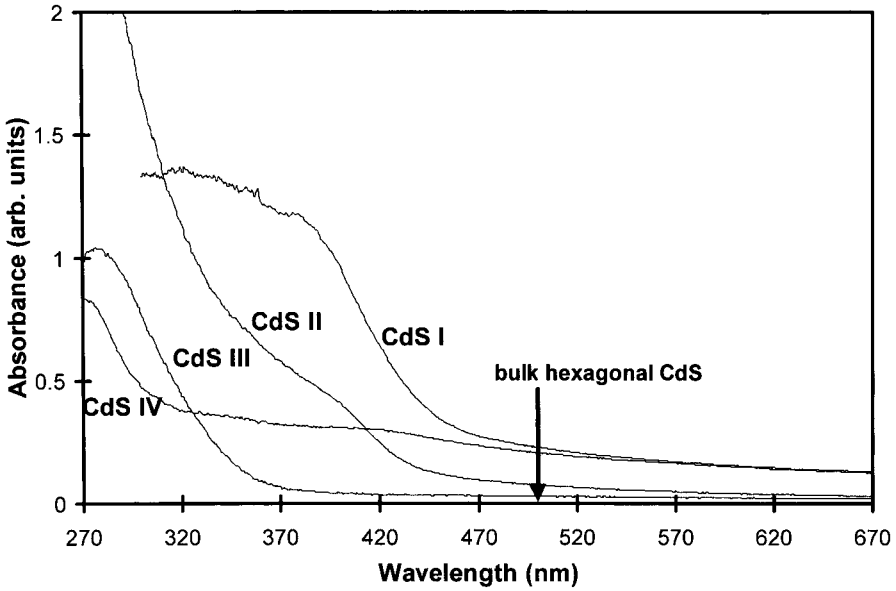

Figure 2. Optical absorption data for CdS-I, CdS-II, CdS-III and CdS-IV samples. All absorption edges are blue-shifted with respect to the band gap of bulk, hexagonal CdS. Note that CdS-II shows two absorption edges corresponding to the cubic and hexagonal phases.

Our data therefore confirm that a size induced hexagonal↔cubic transformation occurs in CdS nanoparticles at about 4.5 nm, which is in excellent agreement with earlier TEM/HREM observations [13]. Assigning the smaller band gap to the cubic phase and the larger band gap to the hexagonal phase is unphysical since it would result in a red-shift of the cubic band gap at smaller particle sizes. The final possibility is that both band gaps in CdS-II correspond to the hexagonal phase with a bimodal size distribution. This requires that CdS-II consist of hexagonal phase particles with sizes of 5.2 nm and 2.6 nm, and implies an unnaturally large size distribution. Further, the presence of 2.6 nm CdS particles in the hexagonal phase would contradict the observation of a hexagonal↔cubic transition at ≈4.5 nm. Thus, our assignment of the smaller band gap in CdS-II to the hexagonal (W) phase and the larger to the cubic (Z) phase is the only self-consistent one. It is also possible for individual CdS particles to consist of mixed phases—as observed by Ricolleau *et al* [14]. This could either arise due to twinning or faulting within a single cubic particle or due to domains of the cubic and hexagonal phase coexisting within the same particle, sharing their respective close-packed planes at the domain boundaries. However, in the present case, the observation of two distinct band gaps (CdS-II) probably implies that the sample consists of distinct particles with the slightly smaller ones having a cubic structure and the larger ones having a hexagonal structure.

4. Discussion

The hexagonal wurtzite and the cubic zinc blende phases of CdS are quite closely related structures and the close-packed planes of these two structures ({0002} in the hexagonal case and {111} in the cubic case) are identical. Both planes exhibit a two-dimensionally projected sixfold symmetry and have the same projected in-plane density of atoms. Both structures consist of periodic stacks of close packed Cd planes with S atoms occupying the fourfold

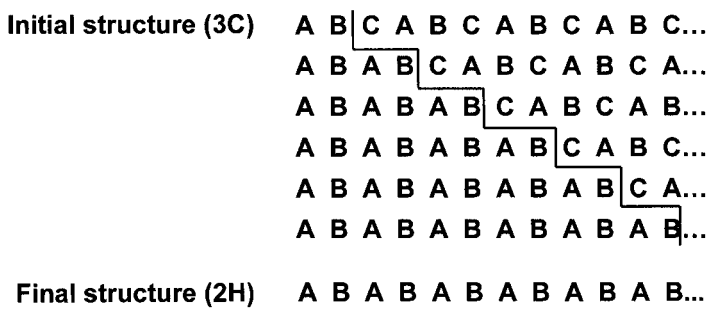

Figure 3. A schematic demonstration of a mechanism involving the introduction of deformation stacking faults on alternate close-packed planes of the parent $3C$ structure, which can transform it completely to the $2H$ structure.

coordinated tetrahedral interstitial sites. The difference between the two structures is only in the stacking sequence of the close-packed planes. The stacking sequence is ABABABA... ($2H$) in the W structure and ABCABCABCA... ($3C$) for the Z structure.

Since the $3C$ and $2H$ structures are polytypic, it is relatively easy to transform one to the other by locally changing the stacking sequence by introducing a series of twins or stacking faults. A single twinned fault introduced into a $3C$ structure results in three layers adopting the $2H$ structure. An intrinsic stacking fault results in four layers taking on the $2H$ structure while an extrinsic stacking fault results in three layers adopting the $2H$ structure [18]. Sebastian *et al* [19] discuss in detail how different stacking fault configurations can occur in ZnS crystals and transform the structure from $2H$ to $3C$. They show that it is the *deformation fault configuration* that is primarily responsible for the structural transition. This is produced by slipping one part of the crystal past another, parallel to the close-packed basal planes of the hexagonal unit cell. The partial slip or displacement vector is $1/3\langle 10\bar{1}0\rangle$ for a parent $2H$ structure, and $1/6\langle 112\rangle$ for a parent $3C$ structure. The partial slip vector moves atoms from an A to a B position, from a B to a C position and from a C to an A position. Deformation stacking faults introduced on alternate close-packed planes of the $3C$ structure can transform it completely to the $2H$ structure. This mechanism is schematically depicted in figure 3. The ease of introducing such stacking faults depends on the stacking fault energy (SFE) of the compound. From a study of the dissociation of dislocations by weak beam TEM, the SFE in CdS was found to be $\sim$8.7 mJ m^{-2} [20]. This is quite low compared to typical semiconductors and metals which have SFEs in the range of 50–150 mJ m^{-2}. The low SFE in CdS implies that the transformation between the cubic and hexagonal phases is energetically feasible. Further, the transformation mechanism involves no distortion in the nearest-neighbour bonds and in the atomic coordination. The mechanism of the wurtzite to rocksalt transformation, proposed by Tolbert and Alivisatos [21] is much more complex and justifies the extreme conditions of high pressure required to induce it.

Note that we observed both the hexagonal and cubic phases in differently sized CdS nanoparticles synthesized under similar conditions. This implies that the formation of cubic CdS is a size effect and not due to a non-equilibrium synthesis process. Note also that the finer-sized cubic CdS nanoparticles were obtained by adding *larger* quantities of surfactant, which *slows down* the precipitation kinetics. The coarser CdS particles, precipitated at higher rates than the finer particles, should—if at all—be expected to show greater non-equilibrium (metastability) effects. But the bulk equilibrium hexagonal phase actually forms in the coarser particles and the cubic phase in the finer ones. This negates the first of the two possible explanations for the formation of cubic CdS (section 1) proposed in [3].

The nucleation and growth of CdS particles from solution is primarily governed by the competition between the surface and volume free energies of the particle. During nucleation, the surface energy contribution dominates, so that reductions in the free surface area and surface energy would be favoured. The free surface area can be minimized by the nucleus adopting a spherical shape (minimal surface/volume). This can be achieved by adopting a crystal structure amenable to the formation of a spherelike nucleus by exposing close-packed low-energy planes as facets on the surface of the nucleus. Symmetry considerations favour the cubic crystal structure over the hexagonal one for the formation of a spheroidal nucleus with a large number of {111} facets on the surface. We therefore expect the CdS nanoparticles to adopt a cubic structure at the initial stage of nucleation and transform to the bulk stable hexagonal structure during growth.

5. Conclusions

With a reduction in the particle size in CdS nanoparticles, there is a transformation from the bulk hexagonal wurtzite-type structure to the cubic zinc-blende-type structure. The critical transformation size is around 4–5 nm. We have been able to distinguish the effect of the size-induced Scherrer broadening from the structural-transformation-induced changes in the x-ray diffraction patterns. Our results indicate that the optical properties of nanocrystalline CdS are governed not only by quantum confinement effects but also by the size-induced structural phase transition. This is also the first attempt to obtain a value for the band gap of the cubic zinc blende structure of CdS, based on the optical and x-ray diffraction data. The observation of two distinct absorption edges in CdS nanoparticles is shown to result from the presence of coexisting cubic and hexagonal phases. We have also presented a simple mechanism for the transformation from the zinc blende to the wurtzite structure, based on periodic insertion of stacking faults.

References

[1] Alivisatos A P 1996 *J. Phys. Chem.* **100** 13 226
[2] Brus L E 1984 *Chem. Phys.* **80** 4403
[3] Bandaranayake R J, Wen G W, Lin J Y, Jiang H K and Sorensen C M 1995 *Appl. Phys. Lett.* **67** 831
[4] Zou B S, Little R B, Wang J P and El-Sayed M A 1999 *Int. J. Quantum Chem.* **72** 439
[5] Danaher W I, Lyons L E and Morris G C 1985 *Solar Energy Mater.* **12** 137
[6] Colvin V L, Schlamp M C and Alivisatos A P 1994 *Nature* **370** 354
[7] Vossmeyer T, Katsikas L, Giersig M, Popovic I G and Weller H 1994 *J. Phys. Chem.* **98** 7665
[8] Villars P and Calvert L D (eds) 1985 *Pearson's Handbook of Crystallographic Data for Intermetallic Phases* vol 2 (Metals Park, OH: ASM International)
[9] Chen C C, Herhold A B, Johnson C S and Alivisatos A P 1997 *Science* **276** 398
[10] Guinier A 1963 *X-Ray Diffraction* (San Francisco: Freeman)
[11] Nanda J, Kuruvilla B A and Sarma D D 1999 *Phys. Rev.* B **59** 7473
[12] Herron N, Wang Y and Eckert H 1990 *J. Am. Chem. Soc.* **112** 1322
[13] Ricolleau C, Audinet L, Gandais M and Gacoin T 1998 *Thin Solid Films* **336** 213
[14] Ricolleau C, Audinet L, Gandais M, Gacoin T, Boilot J P and Chamarro M 1996 *J. Cryst. Growth* **159** 861
[15] Abd-Lefdil S, Messaoudi C, Abd-Lefdil M and Sayah D 1998 *Phys. Status Solidi* a **168** 417
[16] Rachinger W A 1948 *J. Sci. Instrum.* **25** 254
[17] Kayanuma Y 1988 *Phys. Rev.* B **38** 9797
Mandal S K, Chaudhuri S and Pal A K 1999 *Thin Solid Films* **350** 209
[18] Hirth J P and Lothe J 1968 *Theory of Dislocations* (New York: McGraw-Hill) p 288
[19] Sebastian M T, Pandey D and Krishna P 1982 *Phys. Status Solidi* a **71** 633
[20] Takeuchi S and Suzuki K 1999 *Phys. Status Solidi* a **171** 99
[21] Tolbert S H and Alivisatos A P 1995 *J. Chem. Phys.* **102** 4642